A LABORATORY STUDY OF OFFSHORE TRANSPORT OF SEDIMENT AND A MODEL FOR ERODING BEACHES

Tsuguo Sunamura *Institute of Geoscience, University of Tsukuba, Ibaraki 305, Japan*

ABSTRACT

A two-dimensional laboratory investigation of sediment transport, induced by shallow-water waves, showed that the sediment motion over suspension-dominant asymmetric ripples is closely related to the development of eroding beaches. High-speed motion picture analysis revealed that vortices, formed over this type of ripple, play a crucial role in transporting the sediment to the offshore region. A relation for net offshore sediment flux was formulated for sand 0.02 cm in diameter. A simple model for eroding beaches was proposed and its validity was checked by using two existing data sets for 0.02-cm sand beaches; the model could predict fairly well profile and shoreline changes in the early stages.

INTRODUCTION

Shallow-water waves produce a net sediment transport on a beach. Since beach changes do occur only when a spatial difference of net sediment transport rate exists, an explicit understanding of sediment motion under shallow-water wave action is necessary for beach change studies. Although much research on sediment motion has been conducted in the laboratory (e.g., Davies and Wilkinson, 1977), few have focussed attention on this point.

Beach erosion is clearly caused by the net offshore movement of sand. However, the mechanisms of the offshore movement have not yet been fully clarified even in a laboratory environment; so that no models for predicting erosional beaches have been developed on the basis of sediment dynamics.

The present two-dimensional laboratory study attempts to (1) investigate sediment motion by shallow-water waves and relate this to the beach profile change, (2) elucidate the processes of net offshore transport of sand and estimate the transport rate, and (3) develop a simple model for eroding beaches.

SEDIMENT MOVEMENT CAUSED BY SHALLOW-WATER WAVES AND ITS RELATION TO BEACH PROFILE CHANGE

Komar and Millar (1973; 1974) gave the following relation for the sediment threshold, which was a dimensionally corrected Bagnold's (1946) empirical relation:

$$\rho\, u_m^2 \,/\, (\rho_s - \rho)\, g\, D \;=\; a\, (d_o/D)^{1/2} , \tag{1}$$

where u_m = maximum orbital velocity of the water near the bottom, d_o = maximum orbital diameter near the bottom, D = sediment size, ρ_s = sediment density, ρ = water density, g = gravitational acceleration, and a = dimensionless constant. Equation (1) reduces to

$$H_o/L_o \;=\; a' \,(D/L_o)^{1/3}\, (H_o/H)\, \sinh(2\pi h/L) , \tag{2}$$

where $a' = [(2a/\pi)(\rho_s/\rho - 1)]^{2/3}$ = const., using the following relations based on the Airy wave theory:

$$u_m = \pi H / T \sinh(2\pi h/L) , \tag{3}$$

$$d_o = H / \sinh(2\pi h/L) , \tag{4}$$

$$L_o = g\, T^2 / 2\pi, \tag{5}$$

where H and L = wave height and length at a water depth of h, respectively, H_o and L_o = wave height and length in deep water, respectively, and T = wave period. Equation (2) is basically the same relation that Sato et al. (1962) introduced for the description of sediment motion. A theoretical study by Horikawa and Watanabe (1967) indicated that Eq. (2) is valid only for the onset of sediment movement under conditions of a hydralically rough bottom and turbulent boundary layer flow. However, Eq. (1) is in good agreement with Bagnold's (1946) and Manohar's (1955) data obtained under laminar boundary layer flow conditions, although the values of a differ slightly from each other (Komar and Miller, 1973; 1974). A further investigation by Komar and Miller (1975) showed that Eq. (1) can also specify the initiation of ripple formation, which amounts to a change in the value of a. A review of these existing studies suggests that the form of Eq. (1) may be applicable to sediment movement under various flow conditions and also to ripple initiation, although this application is theoretically restricted. A useful dimensionless parameter describing sediment motion and bedform would be

$$F \;=\; \rho\, u_m^2 \,/\, (\rho_s - \rho)\, g\, D^{1/2}\, d_o^{1/2} , \tag{6}$$

which is an algebraic rearrangement of Eq. (1).

Shallow-water waves create a near-bottom velocity field which is characterized by a larger onshore velocity of shorter duration under wave crests, and a smaller offshore velocity of longer duration under wave troughs, as compared to a purely sinusoidal orbital velocity field. A dimensionless parameter on which the deviation from the sinusoidal velocity field depends, is the Ursell number (Ursell, 1953):

$$U = H L^2 / h^3. \tag{7}$$

With increasing U, the degree of deviation becomes greater.

A relationship between F and U (Eqs. (6) and (7)) was investigated on the basis of a laboratory experiment performed using a large (25 m long, 1.5 m deep, and 0.8 m wide) and a small wave tank (6 m long, 0.3 m deep, and 0.2 m wide). Both tanks were equipped with flap-type wave makers at one end of the tank, and wave absorbers were placed at the other end. Four kinds of well-sorted bed material with Trask's (1930) sorting coefficients of 1.05~1.10 were used. Three kinds of sand with the same density, ρ_s = 2.65 g/cm^3, and different diameters, D = 0.02, 0.07, and 0.156 cm, and plastic beads with ρ_s = 1.33 g/cm^3 and D = 0.055 cm were used. A flat horizontal bed was set up in the central portion of the wave tank. Water depth over the horizontal bed was 30~40 cm for the large tank test, and 10~15 cm for the small tank test. Wave period ranged from 1.0~3.4 sec for the former, and 0.69~1.7 sec for the latter. A series of tests was performed by gradually increasing wave height with wave period being kept constant. The mode of sediment motion and bedform were observed visually.

The results are shown in Fig. 1. Different values of k in the following equation gave a fairly good demarcation of the different regions of bedforms:

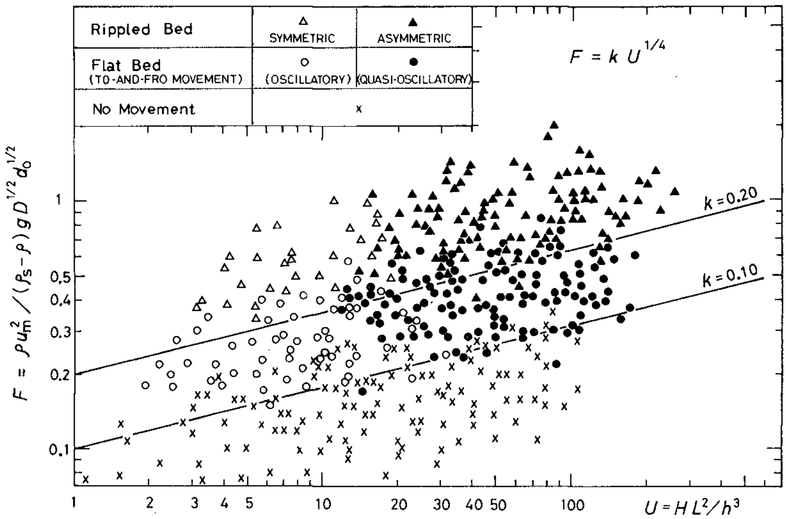

Figure 1. Relationship between F and U for bedfom demarcation.

$$F = k\, U^{1/4} \; . \tag{8}$$

With increasing the Ursell number, either non-sinusoidal sediment movement or asymmetric bedform occurs becoming noticeable for $U \gtrsim 10 \sim 20$. The region occupied by solid circles ($0.10 \lesssim k \lesssim 0.20$) denotes the occurrence of a quasi-oscillatory bedload producing a net onshore transport. Above this region, lies a region of asymmetric ripples, shown by a cluster of solid triangles ($k \gtrsim 0.20$). When ripples are formed, there always exists suspended sediment, which is defined here as the sediment moved not only in pure suspension but also in saltation.

To study sediment motion over asymmetric ripples, Sato and Tanaka (1962) and Sato et al. (1962) have performed radioactive-tagged sand tracer experiments. They replaced the sand forming one asymmetric ripple by radioactive sand and traced its movement. The results demonstrated the occurrence of two different types of sediment motion: one is bedload dominant movement producing a net onshore transport (Fig. 2), while the other is suspended-load dominant movement producing a net offshore transport (Fig. 3). Note that Fig. 3 shows no onshore dispersion of the tracer.

Figure 4 is a plot of selected data showing the directions of net sediment transport over asymmetric ripples; solid symbols denote offshore transport, while open symbols onshore transport. Although there are not a sufficient number of the data points, a boundary between onshore and offshore regions could be expressed by the dashed line:

$$F \;\begin{matrix} > \\ < \end{matrix}\; 0.28\, U^{1/4} \quad \begin{matrix} \text{Net offshore transport} \\ \text{Net onshore transport.} \end{matrix} \tag{9}$$

If this relation is applicable at the wave breaking point of a sloping beach, then the following relation can be written:

$$F_b \gtrless 0.28\, U_b^{1/4} \; . \tag{10}$$

The subscript " b " denotes quantities at the wave breaking point. If the left-hand side of this equation is greater than the right-hand side, then net offshore transport of sediment takes place through the wave breaking point; this leads to the development of an eroding beach as shown in the inset of Fig. 5. For the reverse case, an accreting beach develops. If the preceding assumption is valid, then a boundary between eroding and accreting beaches should be given by

$$F_b = 0.28\, U_b^{1/4} \; , \tag{11}$$

where

$$F_b = \rho\, (u_m)_b^2 \,/\, (\, \rho_s - \rho \,)\, g\, D^{1/2}\, (d_o)_b^{1/2} \; ,$$

$$U_b = H_b\, L_b^2 \,/\, h_b^3 \; ,$$

$$(u_m)_b = \pi\, H_b \,/\, T \sinh(\, 2\pi h_b/L_b \,) \; ,$$

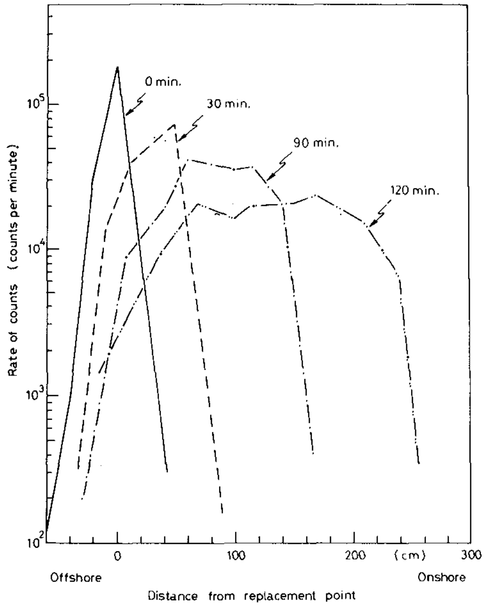

Figure 2.

Temporal change of radioactive sand distribution, showing net onshore transport. (Sato et al., 1962)

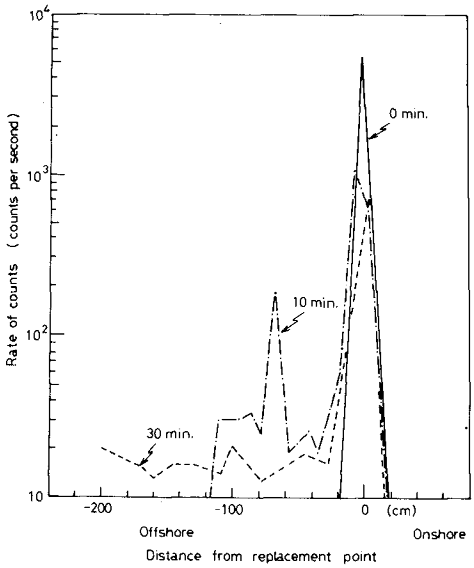

Figure 3.

Temporal change of radioactive sand distribution, showing net offshore transport. (Sato et al., 1962)

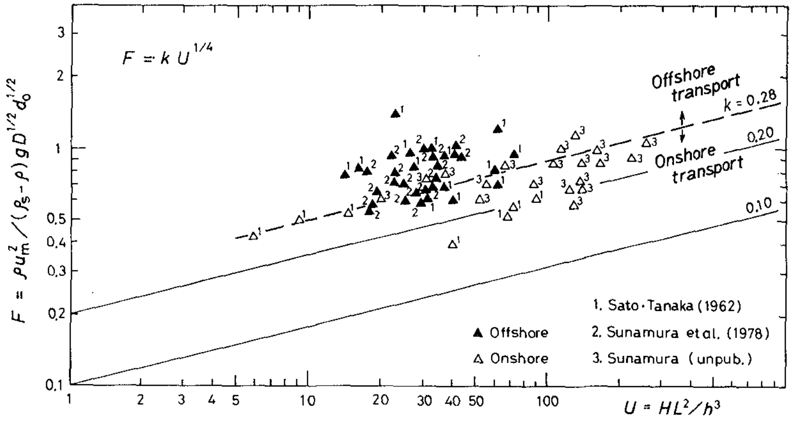

Figure 4. Directions of net sediment-transport over ripples.

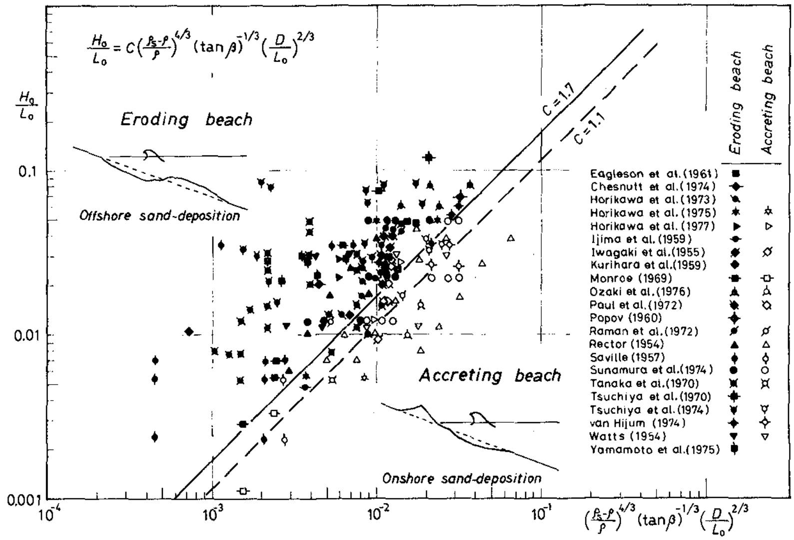

Figure 5. Demarcation of eroding and accreting beaches.

Table 1. Data sets used for the validity check of Eq. (12).

No.	Researcher(s)	D (cm)	ρ_s (g/cm^3)	$\tan\beta$	H_o (cm)	T (sec)	t (hr)	Remarks*
1.	Eagleson et al. (1961)	0.037	2.65	1/20-1/45	9.1-10.8	1.15-1.53	121-222	S, M
2.	Chesnutt et al. (1974)	0.02	2.65	1/10	11.8	1.9	375	S, M
3.	Horikawa et al. (1973)	0.02	2.65	1/24	5.3-7.3	1.4-1.7	48-240	S, M
4.	Horikawa et al. (1975)	0.02-0.07	2.65	1/10	3.4-7.6	1.0-2.0	178-266	S, M
5.	Horikawa et al. (1977)	0.02-0.07	2.65	1/10	7.5-10	1.5-2.0	1-20	S, M
6.	Ijima et al. (1959)	0.028	2.65	1/20	6.8-7.7	1.5-3.0	20-23.3	S, M
7.	Iwagaki et al. (1955)	0.03	2.63	1/10	2.09-5.88	1.07-1.21	4-12	S, M
8.	Kurihara et al. (1959)	0.02 0.03	2.65 1.30	1/10 1/10	3.84 4.30	1.39 1.64	5-7 5-7	S, M C, M
9.	Monroe (1969)	0.027	2.65	1/15	4.33-17.1	1.19-5.06	16-47	S, M
10.	Ozaki et al. (1976)	0.022-0.049	2.65	1/50	4.4-14.4	0.86-1.69	60-128	S, M
11.	Paul et al. (1972)	0.0357-0.063	2.67-2.71	1/10	4.15-18.2	1.29-1.71	≥36	S, M
12.	Popov (1960)	0.6	2.65	1/3	31.3	1.73	16.8	S, M
13.	Raman et al. (1972)	0.03	2.65	1/8-1/15	6.49-7.54	1.0-2.0	40-45	S, M
14.	Rector (1954)	0.022-0.344	2.65	1/30	10.1-13.1	1.3-3.3	70-200	S, M
15.	Saville (1957)	0.022	2.65	1/15	3.05-168	1.77-11.3	40	S, M
16.	Sunamura et al. (1974)	0.02-0.07	2.65	1/10-1/30	3.4-7.6	1.0-2.0	160	S, M
17.	Tanaka et al. (1970)	0.02 0.023	2.65 1.60	1/20 1/10-1/20	3.2-10.8 2.8-10.8	0.95-1.98 0.95-2.2	10-15 10-15	S, M C, M
18.	Tsuchiya et al. (1970)	0.02	2.65	1/15	7.2	0.62	130	S, W
19.	Tsuchiya et al. (1974)	0.022-0.073 0.032	2.59-2.65 1.36	1/15 1/15	2.08-18.7 1.90-14.8	0.76-1.34 0.89-1.27	15-60 7-15	S, W C, W
20.	van Hijum (1974)	0.13-0.61	2.65	1/5-1/10	16.2-38.0	1.6-2	0.5-4	S, M
21.	Watts (1954)	0.022-3.44	2.65	1/20	12.7-18.7	2.0-2.68	40	S, M
22.	Yamamoto et al. (1975)	0.018 0.021	2.65 1.45	1/10-1/50 1/10-1/50	11.4-18.8 2.06-3.59	1.8-2.0 0.8-0.9	10-31.5 4-17	S, M C, M

* S = Sand; C = Coal powder; M = Monochromatic waves; W = Wind waves

$(d_o)_b = H_b / \sinh(2\pi h_b/L_b)$.

Equation (11) was transformed using the approximations: $\sinh(2\pi h_b/L_b) \simeq 2\pi h_b/L_b$, $\tanh(2\pi h_b/L_b) \simeq 2\pi h_b/L_b$, $29/30 \simeq 1$, and $35/12 \simeq 3$; and two empirical relations on breaker characteristics:

$$H_b/h_b = 1.1 (\tan \beta)^{1/6} (H_o/L_o)^{-1/12} , \text{ (see Appendix)} \tag{12a}$$

$$H_b/H_o = (\tan \beta)^{1/5} (H_o/L_o)^{-1/4} , \tag{12b}$$

where $\tan \beta$ = beach slope and Eq. (12b) was given by Sunamura and Horikawa (1974). This results in

$$H_o/L_o = C (\rho_s/\rho - 1)^{4/3} (\tan \beta)^{-1/3} (D/L_o)^{2/3} \tag{13}$$

with the constant, C , being equal to 1.1. The parameters, H_o/L_o and $(\tan \beta)^{-1/3} (D/L_o)^{2/3}$, are very similar to the parameters used for beach profile classification, which were semi-empirically obtained on the basis of surf-zone hydraulics, i.e., H_o/L_o and $(\tan \beta)^{-0.27} (D/L_o)^{0.67}$ (Sunamura and Horikawa, 1974). The validity of Eq. (13) was checked using the existing beach profile data with various wave durations, t (Table 1). The results are plotted in Fig. 5; $C = 1.1$ gives a good demarcation between eroding and accreting beaches, although $C = 1.7$ provides the best. This suggests that the sediment transport mode at the wave breaking point is closely related to beach profile change.

MECHANICS OF OFFSHORE TRANSPORT OF SEDIMENT AND QUANTIFICATION OF TRANSPORT RATE

For the development of a model for eroding beaches, knowledge of net offshore sediment flux, associated with the wave and sediment parameters, is required. Sediment motion producing a net offshore transport is very rapid and complex. This quickness and complexity have hampered this sort of study.

In order to overcome these difficulties, a 16-mm high-speed movie camera was adopted for a laboratory test, in which the small wave tank was used (Sunamura et al., 1978). The movement of the well-sorted 0.02-cm sand, which formed asymmetric ripples with suspension-dominant transport on a horizontal bed, was photographed at a film speed of 200 500 frames/sec. Neutral-buoyant polystyrene beads, 1.5 mm in diameter, were used for tracing the water orbital motion.

Figure 6 shows one characteristic example of sediment movement, taken from the high-speed motion picture films via a film analyzer. The ellipses indicate the orbital motion of the water and the multiple arrows denote sand particle velocity vectors. Note that the sand particles are entrapped in a vortex formed at the onshore side of the R_2 ripple in stage (1); the particles are represented by open circles. Immediately after the onset of offshore flow, these sand particles are

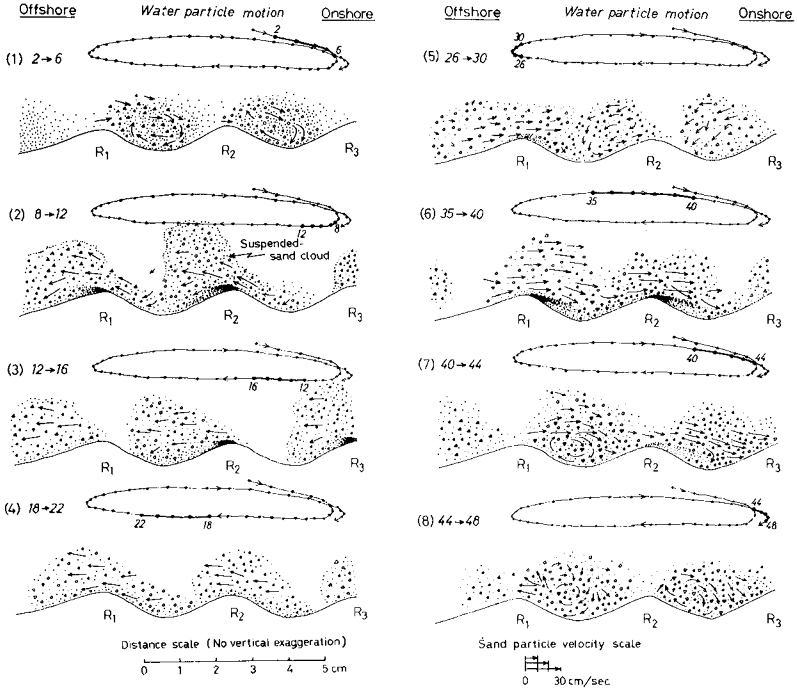

△ : Sand forming the suspended sand cloud initiated at R_1 at the stage between (1) and (2).

○ : 〃 〃 R_2 at the stage (2).

● : 〃 〃 R_3 at the stage between (2) and (3).

▼ : Sand carried from the crest of R_1 by onshore current at the stages (5) and (6).

▽ : 〃 R_2 〃 (6) and (7).

Approximate time interval between consective two dots in water-particle-motion diagrams is 2.9×10^{-2} sec.

Figure 6. Sediment movement over asymmetric ripples with suspension-dominant transport. (Sunamura et al., 1978)

thrown up obliquely in an offshore direction to form a suspended-sand cloud, which is shown in stage (2). The following two stages, (3) and (4), show that the offshore flow carries this sand cloud offshore, partially depositing the sand particles. As shown in stages (5) and (6), the onshore flow returns these offshore-transported sand particles to the place where they were initially entrapped in the vortex, that is, to the onshore side of the R_2 ripple. During this return travel, however, the sediment once transported offshore beyond a certain limit cannot return to the onshore side of the R_2 ripple, due to being captured in a vortex formed at the onshore flank of the R_1 ripple, as shown in stage (7). This unreturned sediment constitutes the net offshore-transported load. It should be emphasized that strong vortices, formed over the onshore flank of asymmetric ripples, play a vital role in continuing the net offshore sediment transport in this mode of suspension. These vortices are formed with an approximate phase lag of $\pi/6$ after the onshore orbital motion attains its maximum speed.

The film analysis indicated that the offshore limit, beyond which offshore-transported sediment never returns to the initial position, is located at 1.5 λ, where λ is the ripple length (Fig. 7). Sediment in the hatched portion constitutes the net offshore-transported load. In this figure, ℓ is the maximum offshore extension of the sand cloud. Precise measurement of this transported load is extremely difficult, because the measurement must be done without disturbing ripple configuration or the velocity field. However, an estimation is possible if we assume a triangular distribution of sediment particles over the ripples at the stage of maximum offshore extension of the sand cloud (Fig. 8). The following relation can be written:

$$Q_{off} = \delta Q , \tag{14}$$

where Q_{off} = net offshore transport volume of sediment, Q = volume of sediment included in a sand cloud, and

$$\delta = \begin{cases} 0 , & \ell \leq 1.5 \lambda \\ (1 - 1.5 \lambda/\ell)^2, & \ell > 1.5 \lambda . \end{cases}$$

The direct measurement of Q is difficult due to the variability of shape and size of the sand cloud. Since the sand cloud originates from the sand vortex, Q is considered to be approximately equal to the volume of sand forming the vortex. During the vortex formation, (1) the area of the vortex only changes a little and (2) the sand distribution within the vortex seems to be uniform. Then, Q can be expressed by

$$Q = A S / T, \tag{15}$$

where A = area of the vortex, S = volumetric sand concentration in the vortex, and T = wave period. In order to relate Q to the parameters associated with the velocity field and sediment characteristics, the following dimensionless quantities are introduced:

$$\Omega = Q / \sqrt{(\rho_s/\rho - 1) g D}\ D \tag{16}$$

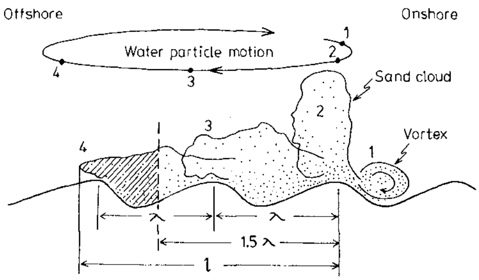

Figure 7.

Definition sketch.

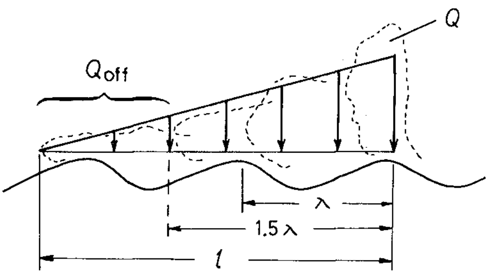

Figure 8.

Definition sketch.

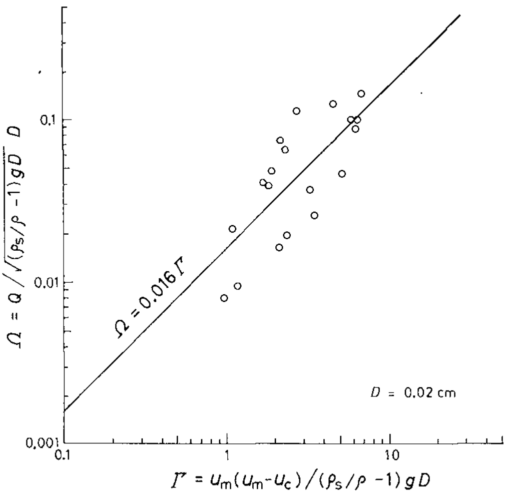

Figure 9.

Relationship between Ω and Γ for 0.02-cm sand.

$\Gamma \ = \ u_m \ (\ u_m - u_c \ ) \ / \ (\ \rho_s/\rho - 1 \ ) \ g \ D \quad \big] \ ,$

where u_c = critical velocity for asymmetric ripple formation = $0.02^{1/2} \cdot (\rho_s/\rho - 1)^{1/2} g^{1/2} D^{1/4} d_o^{1/4} (HL^2/h^3)^{1/8}$; this was obtained by substituting $k = 0.20$ and $u_m = u_c$ into Eq. (8) (see Fig. 1).

To find a connection between Ω and Γ , a laboratory experiment was performed on a horizontal bed, in the small wave tank, made of the well-sorted 0.02-cm sand. The high-speed movie camera was used for the measurement of A . An Iowa-type sediment concentration meter (Locher et al., 1974) was employed to measure S . The measurement, made in the vicinity of the vortex center, was completed within four or five waves, because longer installation of the sensor skewed the ripples so that a change of sand volume in the vortex occurred. For the computation of Q , using Eq. (15), the mean values of A and S were used; the former was averaged over several waves and the latter was a time-averaged value, over three consective waves, of the record during the period of vortex formation. Figure 9 shows the relationship between Ω and Γ . Although some scatter of data points is seen, a linear relation is present:

$$\Omega \ = \ 0.016 \ \Gamma. \tag{17}$$

Using Eqs. (14), (16), and (17), a net offshore sediment flux equation is finally obtained:

$$Q_{off} = 0.016 \left(\frac{\ell - 1.5 \ \lambda}{\ell} \right)^2 \frac{u_m \ (\ u_m - u_c \ ) \ \sqrt{D}}{\sqrt{(\ \rho_s/\rho - 1 \ ) \ g}} \ , \tag{18}$$

which gives volumetric transport rate per unit width. This equation is valid only for $\ell > 1.5 \ \lambda$. It should be noted that this is not a general relation for different sediment sizes, but a relation for only 0.02-cm sand. A generalization must await future studies.

A MODEL FOR ERODING BEACHES

In the two-dimensional laboratory beach changes, a feedback relationship between input waves and the resultant topography usually exists (Fig. 10(a)). Especially, on an eroding beach which is characterized by the sediment accumulation in the offshore region, the wave breaking point shifts offshore in time due to the decrease in water depth accompanying the changes of breaker type and height. This was investigated by Chesnutt and Galvin (1974). Since the formulation of the feedback system seems complicated, the present study attempts to develop a simpler model for eroding beaches, based on an open-loop system (Fig. 10(b)), i.e., the system in which no wave-topography interaction exists. Accordingly, no temporal changes occur in the breaker parameters. We further assume that the sand elevation at the wave breaking point does not change with time. Hence, this model has a time-independent breaking point.

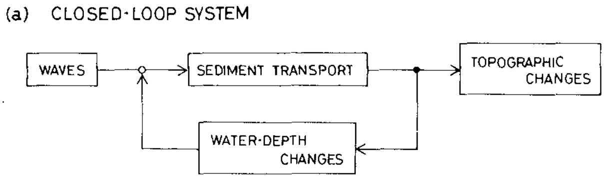

Figure 10. Closed-loop and open-loop systems in beach changes.

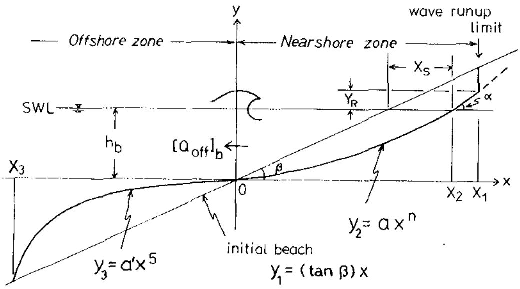

Figure 11.

Definition sketch.

Figure 11 shows the co-ordinate system in which the origin is chosen at the wave breaking point on the initial beach which is expressed by

$$y_1 = (\tan\beta)\, x\,, \tag{19}$$

where $\tan\beta$ = initial beach slope. In the nearshore zone, from the wave breaking point to the wave uprush limit, the eroding beach profile is assumed to be described by

$$y_2 = a\, x^n\,, \tag{20}$$

where both a and n are time-dependent variables. At the wave runup limit, $x = x_1$, the beach profile is expressed by a vertical line or scarp:

$$x_1 = [(h_a + Y_R) / a]^{1/n}\,, \tag{21}$$

where h_b = breaker depth and Y_R = maximum height of wave runup. At the shoreline position, $x = x_2$,

$$(dy_2/dx)_{x = x_2} = \tan \alpha , \tag{22}$$

where $\tan \alpha$ = local beach slope or beach gradient at the shoreline, and

$$x_2 = (h_b / a)^{1/n} . \tag{23}$$

Equations (20), (22), and (23) lead to

$$a = (\tan \alpha)^n / n^n h_b^{n-1} . \tag{24}$$

Since

$$(Q_{off})_b = (1 / t) \int_0^{x_1} (y_1 - y_2) dx , \tag{25}$$

where $(Q_{off})_b$ = net offshore sediment transport rate at the wave breaking point, substitution of Eqs. (19), (20), and (21) into Eq. (25) gives

$$\frac{\tan \beta}{2} \left(\frac{h_b + Y_R}{a} \right)^{2/n} - \frac{a}{n + 1} \left(\frac{h_b + Y_R}{a} \right)^{(n+1)/n} = (Q_{off})_b \cdot t . \tag{26}$$

From Eqs. (24) and (26), both a and n are respectively obtainable as a function of time. Thus, the nearshore beach profile changes can be described by Eq. (20). The shoreline displacement, X_s (see Fig. 11), is given as

$$X_s = \begin{cases} 0 , & (h_b / a)^{1/n} \leq (h_b / \tan \beta) \\ (h_b / a)^{1/n} - (h_b / \tan \beta), & (h_b / a)^{1/n} > (h_b / \tan \beta). \end{cases} \tag{27}$$

In the offshore zone beyond the wave breaking point, $x < 0$ (see Fig. 11), the depositional topography is assumed to be simply given by

$$y_3 = a' x^5 , \tag{28}$$

where a' is a time-dependent variable. Since

$$(Q_{off})_b = (1 / t) \int_{x_3}^{0} (y_3 - y_1) dx, \tag{29}$$

where $x_3 = - [(\tan \beta)/a']^{1/4}$, Eqs. (19), (28), and (29) give the offshore beach profile as

$$y_3 = (\tan \beta)^3 x^5 / 9 (Q_{off})_b^2 t^2 . \tag{30}$$

If the direct application of Eq. (18) is possible to the wave breaking point on a sloping beach made of 0.02-cm sand, then

$$(Q_{off})_b = 0.016 \left(\frac{\ell_b - 1.5 \lambda_b}{\ell_b} \right)^2 \frac{(u_m)_b [(u_m)_b - (u_c)_b] \sqrt{D}}{\sqrt{(\rho_s/\rho - 1) g}}, \quad (31)$$

where ℓ_b = maximum offshore extension of suspended sand cloud at the wave breaking point, λ_b = length of sand ripples formed at the wave breaking point, and

$$(u_c)_b = 0.20^{1/2} \left(\frac{\rho_s - \rho}{\rho} \right)^{1/2} g^{1/2} D^{1/4} (d_o)_b{}^{1/4} \left(\frac{H_b L_b{}^2}{h_b{}^3} \right)^{1/8} .$$

Knowing the four quantities, $\tan \alpha$, Y_R , ℓ_b , and λ_b , it is possible to calculate beach profile changes and shoreline displacements. However, these quantities must be experimentally determined at present.

Table 2 shows the data for two selected experiments with eroding beaches, which was used for a check of the validity of this model. The selection was based on the following three criteria: (1) the grain size of sand used should be 0.02 cm, because the sediment flux equation is available for only 0.02-cm sand; (2) the duration of wave action should be more than 100 hours, because the longer the duration, the better is the check of the characteristics of this model; and (3) data of temporal changes of the beach profile and shoreline position should be available.

A similar experiment on a sloping beach was carried out under the same conditions as listed in the upper rows of Table 2, for only first hour. A flap-type wave maker-equipped tank 16 m long, 0.7 m high, and 0.5 m wide, was used. The four quantities were measured immediately

Table 2. Data sets used for the validity check of the model.

	Chesnutt·Galvin (1974) Experiment No.1-06	Sunamura·Horikawa (1974) Case 4
D	0.02 cm	0.02 cm
$\tan\beta$	0.1	0.1
H_o	11.8 cm	7.6 cm
T	1.9 sec	1.0 sec
t	375 hr	160 hr
λ_b*	11 cm	5 cm
l_b*	$\approx 2.3 \lambda_b$	$\approx 2.3 \lambda_b$
Y_R*	8 cm	4 cm
$\tan\alpha$*	0.12	0.12

* Measured immediately after 30-minute wave action

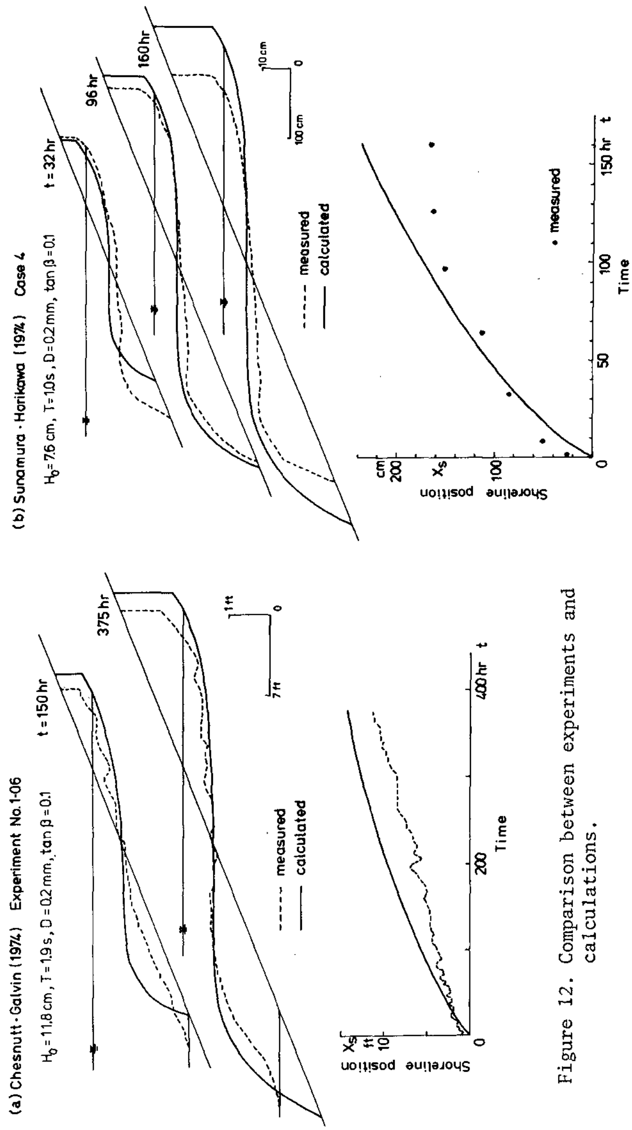

Figure 12. Comparison between experiments and calculations.

after 30 minutes of wave action; the results are listed in the lower rows of Table 2. Assuming these quantities are all independent of time, a calculation was done with breaker characteristics obtained from Eqs. (12a) and (12b).

Figure 12(a) shows that the calculation overestimates the nearshore zone profile, and that the calculation and the experiment are in fairly good agreement only in the early stages. A noticeable disagreement is evident in the mid-late stage. Both the nearshore beach profile and the shoreline changes in Fig. 12(b) show that the calculation and the experiment are in good agreement during the early stages. However, the disagreement becomes marked after these stages, like the result of the former case. One of the reasons for this would probably be the neglect of the effect of wave-topography interaction. Some modification of this model is therefore needed.

CONCLUSIONS

Vortices formed over asymmetric ripples with suspension-dominant transport play a vital role in continuing a net offshore sand transport in this mode of suspension. A validity check using two existing data sets indicates that the eroding-beach model worked fairly well in predicting the erosional features in the early stages.

ACKNOWLEDGMENTS

The horizontal-bed experiments were performed while the author was at the Coastal Engineering Laboratory, University of Tokyo; the supplementary experiment on a sloping beach was conducted using the facilities of the Environmental Research Center, University of Tsukuba. This study was partly supported through the Science Research Fund of the Ministry of Education.

REFERENCES

Bagnold, R. A. (1946): Motion of waves in shallow water; interaction between waves and sand bottoms. Proc. Royal Soc. London, v.187, Series A, p.1-15.

Battjes, J. A. (1974): Surf similarity. Proc. 14th Conf. Coastal Eng., p.466-480.

Chesnutt, C. B. and Galvin, C. J., Jr. (1974): Lab profile and reflection changes for H_o/L_o = 0.02. Proc. 14th Conf. Coastal Eng., p. 958-977.

Davies, A. G. and Wilkinson, R. H. (1977): The movement of non-cohesive sediment by surface water waves, Part I: Literature survey. Inst. Oceanogr. Sci., Report 45, 73 p. (unpub. manuscript).

Eagleson, P. S., Glenne, B. and Dracup, J. A. (1961): Equilibrium characteristics of sand beaches in the offshore zone. U.S. Army Beach Erosion Board, Tech. Memo. 126, 66p.

Horikawa, K. and Watanabe, A. (1967): A study on sand movement due to wave action. Coastal Eng. Japan, v.10, p.39-57.

Horikawa, K., Sunamura, T. and Kitoh, H. (1973): A study of beach deformation by wave action. Proc. 20th Japan. Conf. Coastal Eng., p. 357-363 (in Japanese).

Horikawa, K., Sunamura, T. and Shibayama, T. (1977): Experimental study of two-dimensional shore transformation — Methods for measurement of sand transport rate in offshore region —. Proc. 24th Japan. Conf. Coastal Eng., p.170-174 (in Japanese).

Horikawa, K., Sunamura, T., Kondo, K. and Okada, S. (1975): Experimental study of two-dimensional shoreline change due to waves. Proc. 22nd Japan. Conf. Coastal Eng., p.329-334 (in Japanese).

Ijima, T. and Aono, M. (1959): The effect of sediment size on beach profile change. Proc. 6th Japan. Conf. Coastal Eng., p.49-56 (in Japanese).

Iwagaki, Y. and Sawaragi, T. (1955): An experiment of equilibrium beach profile and sand movement by waves. Proc. 2nd Japan. Conf. Coastal Eng., p.99-105 (in Japanese).

Komar, P. D. and Miller, M. C. (1973): The threshold of sediment movement under oscillatory water waves. Jour. Sed. Petrology, v.43, p.1101-1110.

Komar, P. D. and Miller, M. C. (1974): Sediment threshold under oscillatory waves. Proc. 14th Conf. Coastal Eng., p.756-775.

Komar, P. D. and Miller, M. C. (1975): The initiation of oscillatory ripple marks and the development of plane-bed at high shear stress under waves. Jour. Sed. Petrology, v.45, p.697-703.

Kurihara, M., Shinohara, K., Tsubaki, T. and Yoshioka, M. (1956): Beach sediment movement by waves. Proc. 3rd Japan. Conf. Coastal Eng., p.151-158 (in Japanese).

Locher, F. A., Glover, J. R. and Nakato, T. (1974): Investigation of the operating characteristics of the Iowa sediment concentration measuring system. Iowa Inst. Hydraulic Res., Univ. Iowa, Report 170, 99p.

Manohar, M. (1955): Mechanics of bottom sediment movement due to wave action. U.S. Army Beach Erosion Board, Tech. Memo. 75, 121p.

Monroe, F. F. (1969): Oolitic aragonite and quartz sand: laboratory comparison under wave action. U.S. Army Coastal Eng. Res. Center, Misc. Paper 1-69, 22p.

Ozaki, A. and Watanabe, H. (1976): Scale effect in the experiment of two-dimensional beach profile changes. Proc. 23rd Japan. Conf. Coastal Eng., p.200-205 (in Japanese).

Paul, M. J., Kamphuis, J. W. and Brebner, A. (1972): Similarity of equilibrium beach profiles. Proc. 13th Conf. Coastal Eng., p. 1217-1236.

Popov, I. J. (1960): Experimental research in formation by waves of stable profiles of upstream faces of earth dams and reservoir shores. Proc. 7th Conf. Coastal Eng., p.282-293.

Raman, H. and Earattupuzha, J. J. (1972): Equilibrium conditions in beach wave interaction. Proc. 13th Conf. Coastal Eng., p.1237-1256.

Rector, R. L. (1954): Laboratory study of equilibrium profiles of beaches, U.S. Army Beach Erosion Board, Tech. Memo. 41, 38 p.
Sato, Sh. and Tanaka, N. (1962): Wave induced sand movement on a horizontal bed. Proc. 9th Japan. Conf. Coastal Eng., p.95-100 (in Japanese).
Sato, Sh., Ijima, T. and Tanaka, N. (1962): A study of critical depth and mode of sand movement using radioactive glass sand. Proc. 8th Conf. Coastal Eng., p.304-323.
Saville, T., Jr. (1957): Scale effects in two dimensional beach studies. Proc. 7th Meeting Int. Assoc. Hydraulic Res., p.(A3)1-8.
Sunamura, T. and Horikawa, K. (1974): Two-dimensional beach transformation due to waves. Proc. 14th Conf. Coastal Eng., p.920-938.
Sunamura, T., Bando, K., and Horikawa, K. (1978): An experimental study of sand transport mechanisms and transport rate over asymmetric sand ripples. Proc. 25th Japan. Conf. Coastal Eng., p.250-254 (in Japanese).
Tanaka, N. and Sinbo, O. (1973): Properties of coal grains as bed material in the model experiment on littoral drift. Port and Harbour Res. Inst., Report 12, p.3-57 (in Japanese).
Trask, P. D. (1930): Mechanical analysis of sediments by centrifuge. Econ. Geol., v.25, p.581-599.
Tsuchiya, Y. and Yoshioka, S. (1970): Experimental study of beach deformation by wind waves (1). Memoir 25th Annual Conv., Japan. Soc. Civil Eng., p.97-98 (in Japanese).
Tsuchiya, Y. and Inada, K. (1974): Laboratory experiment of beach changes due to wind waves. Proc. 21st Japan. Conf. Coastal Eng., p.219-224 (in Japanese).
Ursell, F. (1953): The long-wave paradox in the theory of gravity waves. Proc. Cambridge Phil. Soc., v.49, p.685-694.
Van Hijum, E. (1974): Equilibrium profiles of coarse material under wave attack. Proc. 14th Conf. Coastal Eng., p.939-957.
Watts, G. M. (1954): Laboratory study of effect of varying wave period on beach profiles. U.S. Army Beach Erosion Board, Tech. Memo. 53, 19p.
Yamamoto, K. and Nozumi, M. (1975): A study of similarity law in beach changes. Public Works Res. Inst., Tech. Memo. 975, 131p. (in Japanese).

APPENDIX

Figure A-1 is taken from Battjes (1974), in which γ_b = ratio of breaker height to depth = H_b/h_b , and ξ_o = surf similarity parameter = tan β / (H_o/L_o)$^{1/2}$. He stated that $\gamma_b \approx 0.8$ for $\xi_o \leq 0.2$ and that γ_b increases slightly with increasing ξ_o for $\xi_o > 0.2$. However, such a general tendency as indicated by the dashed line (drawn by the present author) is clearly seen in sipte of the considerable scatter of the data points. This line is expressed by

$$\gamma_b = 1.1\ \xi_o^{1/6}$$

or

$$H_b/h_b = 1.1\ (\tan\beta)^{1/6}\ (H_o/L_o)^{-1/12} .$$

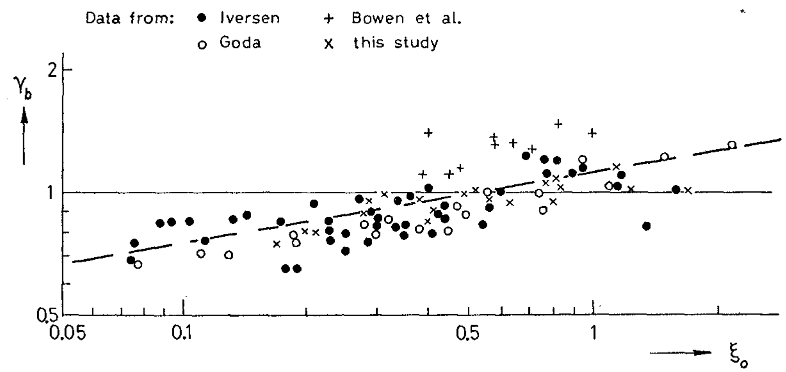

Figure A-1. Breaker height-depth ratio vs. surf similarity parameter (Battjes, 1974).